Supplemental material: Measurement of the electron charge asymmetry in $p\bar{p} \to W + X \to e\nu + X$ events at $\sqrt{s} = 1.96$ TeV

(Dated: May 5, 2015)

The measurement of the electron charge asymmetry in W boson decays [1] has been amended by an erratum [2] to correct the correlation coefficients of systematic uncertainties that were shown in the original publication as the square roots of the calculated values. In the corrected correlation matrices in [2], the component due to the migration of events across bins in electron pseudorapidity, η^ℓ, was calculated using 100% correlations between $|\eta^\ell|$ bins. An alternative choice, preferred by some PDF fitting collaborations, is to take the migration uncertainty as uncorrelated since this uncertainty is dominated by Monte Carlo statistical fluctuations. Tables I to V show the full systematic correlation matrices for the different electron and $\not\!\!E_T$ selections with an uncorrelated migration matrix uncertainty. The $|\eta^\ell|$ bins are defined in the published paper [1].

It is important to demonstrate the level of agreement among the recent Tevatron measurements of the lepton charge asymmetry. Here we provide such comparisons for the lepton charge asymmetries in the published electron channel from D0 [1] (9.7 fb^{-1}), the published muon channel from D0 [3] (7.3 fb^{-1}), and an unpublished electron channel result from CDF [4] (1.0 fb^{-1}). The CDF results are shown with statistical uncertainties only. Figures 1-4 show the measured asymmetries and the differences between the measurements and the prediction of MC@NLO with NNPDF2.3 PDFs [5] for the kinematic regions

1. $E_T^\ell > 25$ GeV and $\not\!\!E_T > 25$ GeV,
2. $25 < E_T^\ell < 35$ GeV and $\not\!\!E_T > 25$ GeV,
3. $E_T^\ell > 35$ GeV and $\not\!\!E_T > 25$ GeV,
4. $E_T^\ell > 35$ GeV and $\not\!\!E_T > 35$ GeV.

Figures 1-4 also show the predictions from other generator/PDF choices. Figures 5-8 show the same distributions but the measurements are only compared to MC@NLO using NNPDF2.3 PDF set.

In region (1) the measurements are in reasonable agreement with theoretical predictions and with each other, apart from the CDF point at the highest $|\eta^\ell|$. In regions (2) and (3), the D0 and CDF measurements in the electron channel agree with each other but disagree with most theoretical predictions. No D0 muon channel measurement is available in this region. In region (4), the D0 electron and muon channel measurements agree with each other but disagree with the predictions. No CDF electron channel measurement is available in this region.

[1] V. M. Abazov *et al.* (D0 Collaboration), Phys. Rev. D **91**, 032007 (2015).

[2] V. M. Abazov *et al.* (D0 Collaboration), Phys. Rev. D **91**, 079901 (2015).

[3] V. M. Abazov *et al.* (D0 Collaboration), Phys. Rev. D **88**, 091102 (R) (2013).

[4] T. Aaltonen *et al.* (CDF Collaboration), http://www-cdf.fnal.gov/physics/ewk/2009/WChargeAsym/

[5] R. D. Ball *et al.*, Nucl. Phys. **B867**, 244 (2013).

[6] S. Frixione and B. R. Webber, J. High Energy Phys. **06**, 029 (2002).

[7] A.D. Martin, W. J. Stirling, R. S. Thorne, and G. Watt, Eur. Phys. J. C **63**, 189 (2009).

[8] C. Balazs and C. P. Yuan, Phys. Rev. D **56**, 5558 (1997).

[9] J. Pumplin, D. R. Stump, J. Huston, H.-L. Lai, P. Nadolsky, and W.-K. Tung, J. High Energy Phys. **07** 012 (2002); D. Stump, J. Huston, J. Pumplin, W.-K Tung, H.-L. Lai, S. Kuhlmann, and J. F. Ownes, J. High Energy Phys. **10**, 046 (2003).

TABLE I: Correlation matrix of the systematic uncertainties between different $|\eta^e|$ bins for events with $E_T^e > 25$ GeV, $\not{E}_T > 25$ GeV. The uncertainty associated with the bin migration is considered uncorrelated between $|\eta^e|$ bins. The "$|\eta^e|$ bin" represents the indexing of the η^e bins used in this analysis.

$\|\eta^e\|$ bin	1	2	3	4	5	6	7	8	9	10	11	12	13
1	1.00	0.24	0.28	0.32	0.32	0.32	0.33	0.30	0.27	0.21	0.14	0.14	0.09
2		1.00	0.56	0.60	0.61	0.61	0.63	0.60	0.53	0.40	0.28	0.28	0.17
3			1.00	0.71	0.72	0.71	0.74	0.68	0.60	0.47	0.32	0.32	0.20
4				1.00	0.84	0.81	0.83	0.67	0.60	0.49	0.33	0.33	0.22
5					1.00	0.83	0.85	0.69	0.62	0.50	0.34	0.34	0.23
6						1.00	0.84	0.72	0.65	0.51	0.35	0.35	0.22
7							1.00	0.78	0.70	0.55	0.38	0.37	0.23
8								1.00	0.77	0.56	0.39	0.38	0.19
9									1.00	0.51	0.35	0.34	0.17
10										1.00	0.26	0.25	0.14
11											1.00	0.18	0.09
12												1.00	0.09
13													1.00

TABLE II: Correlation matrix of the systematic uncertainties between different $|\eta^e|$ bins for events with $25 < E_T^e < 35$ GeV, $\not{E}_T > 25$ GeV. The uncertainty associated with the bin migration is considered uncorrelated between $|\eta^e|$ bins. The "$|\eta^e|$ bin" represents the indexing of the η^e bins used in this analysis.

$\|\eta^e\|$ bin	1	2	3	4	5	6	7	8	9	10	11	12	13
1	1.00	0.02	0.03	0.04	0.04	0.04	0.04	0.03	0.03	0.03	0.02	0.03	0.02
2		1.00	0.15	0.20	0.20	0.17	0.14	0.13	0.12	0.12	0.10	0.13	0.08
3			1.00	0.27	0.27	0.23	0.20	0.20	0.19	0.19	0.15	0.17	0.11
4				1.00	0.39	0.33	0.31	0.28	0.26	0.25	0.20	0.26	0.17
5					1.00	0.37	0.36	0.27	0.22	0.24	0.19	0.28	0.18
6						1.00	0.35	0.27	0.22	0.22	0.18	0.26	0.17
7							1.00	0.31	0.25	0.23	0.17	0.27	0.18
8								1.00	0.32	0.27	0.18	0.23	0.16
9									1.00	0.29	0.18	0.19	0.15
10										1.00	0.17	0.19	0.14
11											1.00	0.14	0.10
12												1.00	0.14
13													1.00

TABLE III: Correlation matrix of the systematic uncertainties between different $|\eta^e|$ bins for events with $25 < E_T^e < 35$ GeV, $25 < \not{E}_T < 35$ GeV. The uncertainty associated with the bin migration is considered uncorrelated between $|\eta^e|$ bins. The "$|\eta^e|$ bin" represents the indexing of the η^e bins used in this analysis.

$\|\eta^e\|$ bin	1	2	3	4	5	6	7	8	9	10	11	12	13
1	1.00	0.05	0.07	0.09	0.08	0.07	0.08	0.08	0.10	0.09	0.07	0.09	0.06
2		1.00	0.17	0.22	0.21	0.18	0.19	0.21	0.24	0.23	0.17	0.21	0.15
3			1.00	0.26	0.26	0.22	0.22	0.26	0.30	0.28	0.21	0.25	0.18
4				1.00	0.33	0.29	0.31	0.32	0.38	0.36	0.27	0.35	0.24
5					1.00	0.31	0.34	0.33	0.37	0.37	0.28	0.37	0.24
6						1.00	0.33	0.29	0.32	0.32	0.25	0.35	0.22
7							1.00	0.31	0.33	0.34	0.28	0.40	0.26
8								1.00	0.36	0.35	0.26	0.34	0.22
9									1.00	0.41	0.30	0.38	0.26
10										1.00	0.30	0.38	0.26
11											1.00	0.30	0.20
12												1.00	0.27
13													1.00

TABLE IV: Correlation matrix of the systematic uncertainties between different $|\eta^e|$ bins for events with $E_T^e > 35$ GeV, $\not{E}_T > 25$ GeV. The uncertainty associated with the bin migration is considered uncorrelated between $|\eta^e|$ bins. The "$|\eta^e|$ bin" represents the indexing of the η^e bins used in this analysis.

$\|\eta^e\|$ bin	1	2	3	4	5	6	7	8	9	10	11	12	13
1	1.00	0.27	0.32	0.35	0.35	0.34	0.36	0.35	0.29	0.26	0.19	0.13	0.09
2		1.00	0.64	0.65	0.65	0.65	0.66	0.69	0.62	0.51	0.37	0.26	0.18
3			1.00	0.77	0.77	0.78	0.80	0.82	0.73	0.61	0.44	0.31	0.21
4				1.00	0.87	0.85	0.88	0.84	0.70	0.64	0.48	0.31	0.21
5					1.00	0.86	0.88	0.84	0.70	0.64	0.48	0.31	0.21
6						1.00	0.86	0.85	0.72	0.64	0.47	0.31	0.21
7							1.00	0.87	0.73	0.65	0.49	0.32	0.22
8								1.00	0.80	0.67	0.48	0.33	0.23
9									1.00	0.59	0.41	0.30	0.21
10										1.00	0.36	0.25	0.17
11											1.00	0.18	0.12
12												1.00	0.09
13													1.00

TABLE V: Correlation matrix of the systematic uncertainties between different $|\eta^e|$ bins for events with $E_T^e > 35$ GeV, $\not{E}_T > 35$ GeV. The uncertainty associated with the bin migration is considered uncorrelated between $|\eta^e|$ bins. The "$|\eta^e|$ bin" represents the indexing of the η^e bins used in this analysis.

$\|\eta^e\|$ bin	1	2	3	4	5	6	7	8	9	10	11	12	13
1	1.00	0.06	0.09	0.11	0.12	0.11	0.13	0.13	0.10	0.07	0.05	0.03	0.02
2		1.00	0.26	0.31	0.34	0.30	0.34	0.35	0.27	0.18	0.13	0.06	0.04
3			1.00	0.47	0.51	0.46	0.51	0.54	0.40	0.27	0.19	0.09	0.06
4				1.00	0.61	0.55	0.61	0.63	0.47	0.32	0.23	0.11	0.08
5					1.00	0.60	0.67	0.69	0.51	0.35	0.25	0.13	0.09
6						1.00	0.60	0.61	0.46	0.32	0.23	0.12	0.08
7							1.00	0.68	0.51	0.36	0.26	0.15	0.09
8								1.00	0.54	0.37	0.26	0.13	0.09
9									1.00	0.28	0.20	0.11	0.07
10										1.00	0.15	0.09	0.06
11											1.00	0.08	0.05
12												1.00	0.04
13													1.00

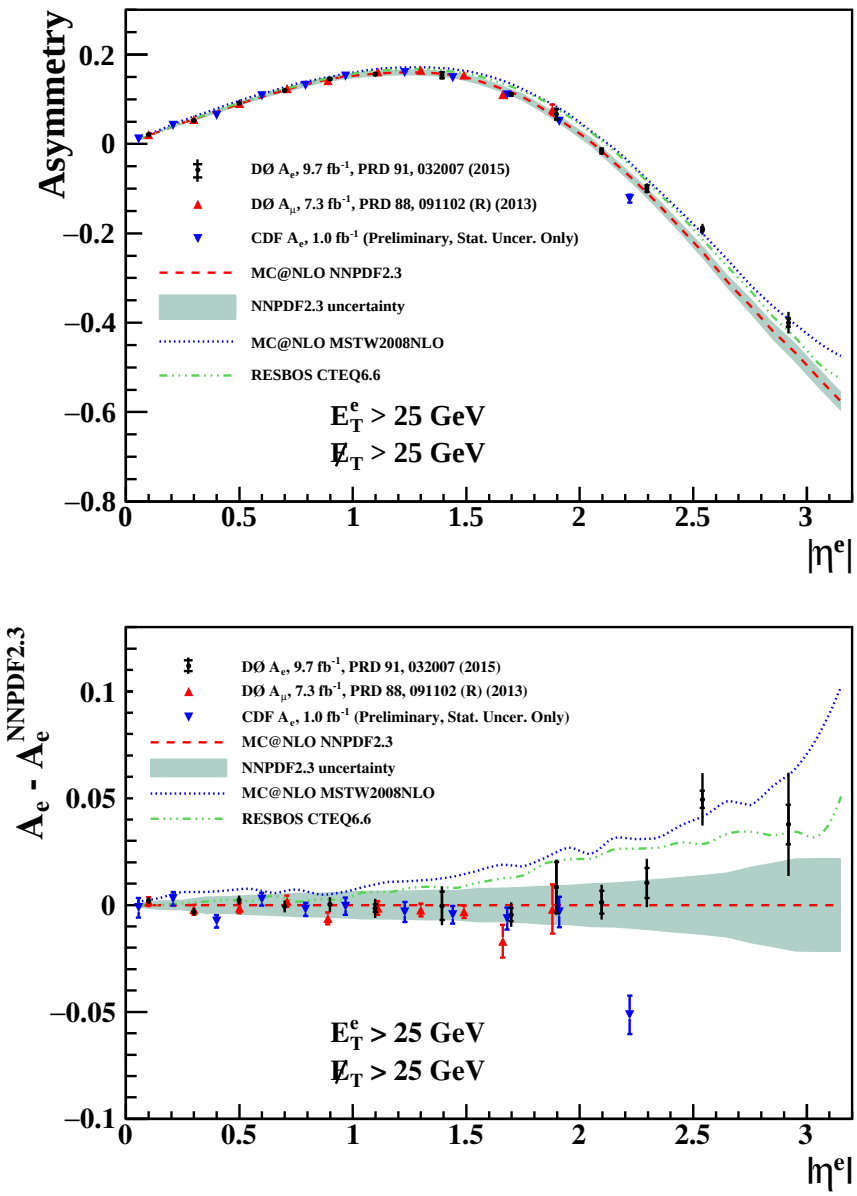

FIG. 1: The electron charge asymmetry distribution after CP folding with symmetric kinematic cuts $E_T^e > 25$ GeV, $\not{E}_T > 25$ GeV. (top) Comparison between the measured asymmetry and predictions and (bottom) the differences between the data and MC predictions and the predicted central value from MC@NLO [6] using the NNPDF2.3 PDF set. The black dots show the measured electron charge asymmetry, with the horizontal bars showing statistical uncertainty and the vertical lines showing the total uncertainty. The red up-pointing triangles show the D0 muon charge asymmetry, the blue down-pointing triangles show the CDF electron charge asymmetry. The red dashed lines and cyan bands are the central value and uncertainty band from MC@NLO using the NNPDF2.3 PDF sets. The blue dotted lines show the prediction from MC@NLO using the MSTW2008NLO [7] central PDF set, and the green dot-dashed lines show the prediction from RESBOS [8] using the CTEQ6.6 [9] central PDF set.

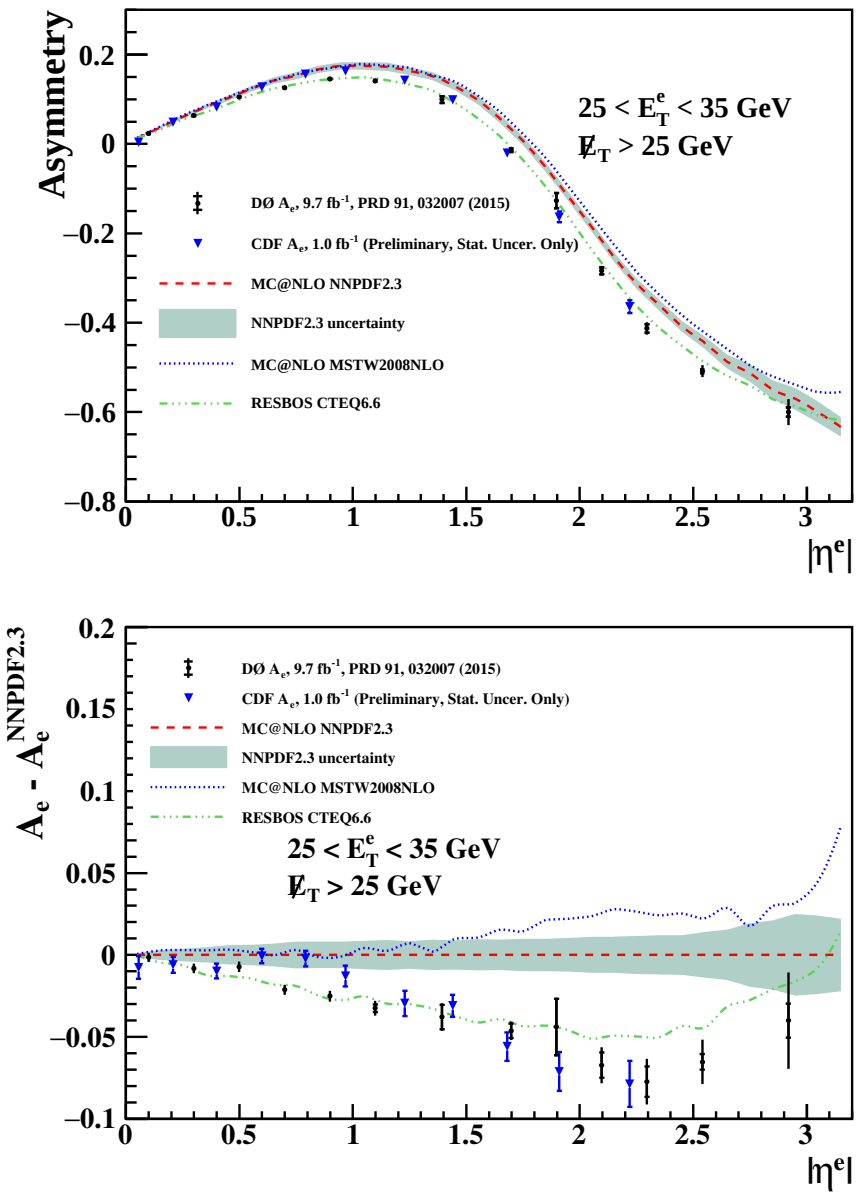

FIG. 2: The electron charge asymmetry distribution after CP folding with symmetric kinematic cuts $25 < E_T^e < 35$ GeV, $\not{E}_T > 25$ GeV. (top) Comparison between the measured asymmetry and predictions and (bottom) the differences between the data and MC predictions and the predicted central value from MC@NLO using the NNPDF2.3 PDF set. The black dots show the measured electron charge asymmetry, with the horizontal bars showing statistical uncertainty and the vertical lines showing the total uncertainty. The blue down-pointing triangles show the CDF electron charge asymmetry. The red dashed lines and cyan bands are the central value and uncertainty band from MC@NLO using the NNPDF2.3 PDF sets. The blue dotted lines show the prediction from MC@NLO using the MSTW2008NLO central PDF set, and the green dot-dashed lines show the prediction from RESBOS using the CTEQ6.6 central PDF set.

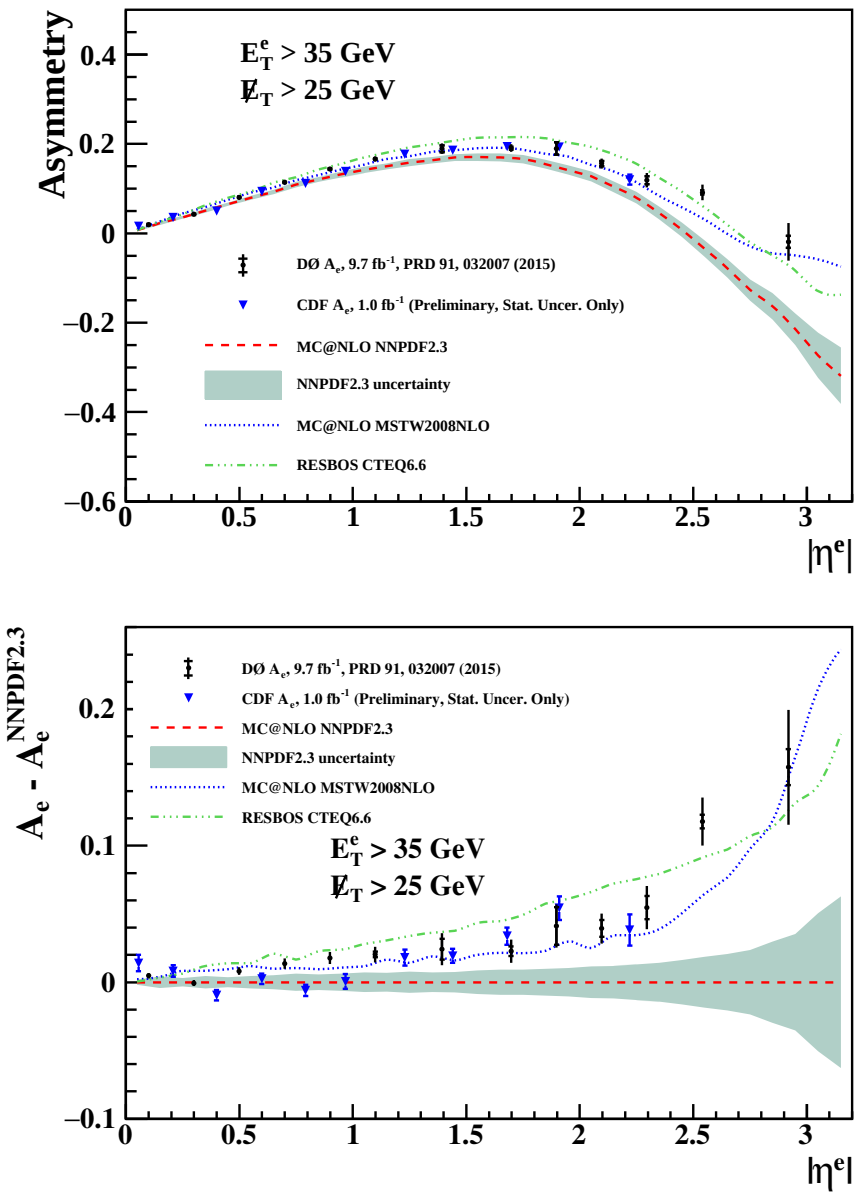

FIG. 3: The electron charge asymmetry distribution after CP folding with symmetric kinematic cuts $E_T^e > 35$ GeV, $\not{E}_T > 25$ GeV. (top) Comparison between the measured asymmetry and predictions and (bottom) the differences between the data and MC predictions and the predicted central value from MC@NLO using the NNPDF2.3 PDF set. The black dots show the measured electron charge asymmetry, with the horizontal bars showing statistical uncertainty and the vertical lines showing the total uncertainty. The blue down-pointing triangles show the CDF electron charge asymmetry. The red dashed lines and cyan bands are the central value and uncertainty band from MC@NLO using the NNPDF2.3 PDF sets. The blue dotted lines show the prediction from MC@NLO using the MSTW2008NLO central PDF set, and the green dot-dashed lines show the prediction from RESBOS using the CTEQ6.6 central PDF set.

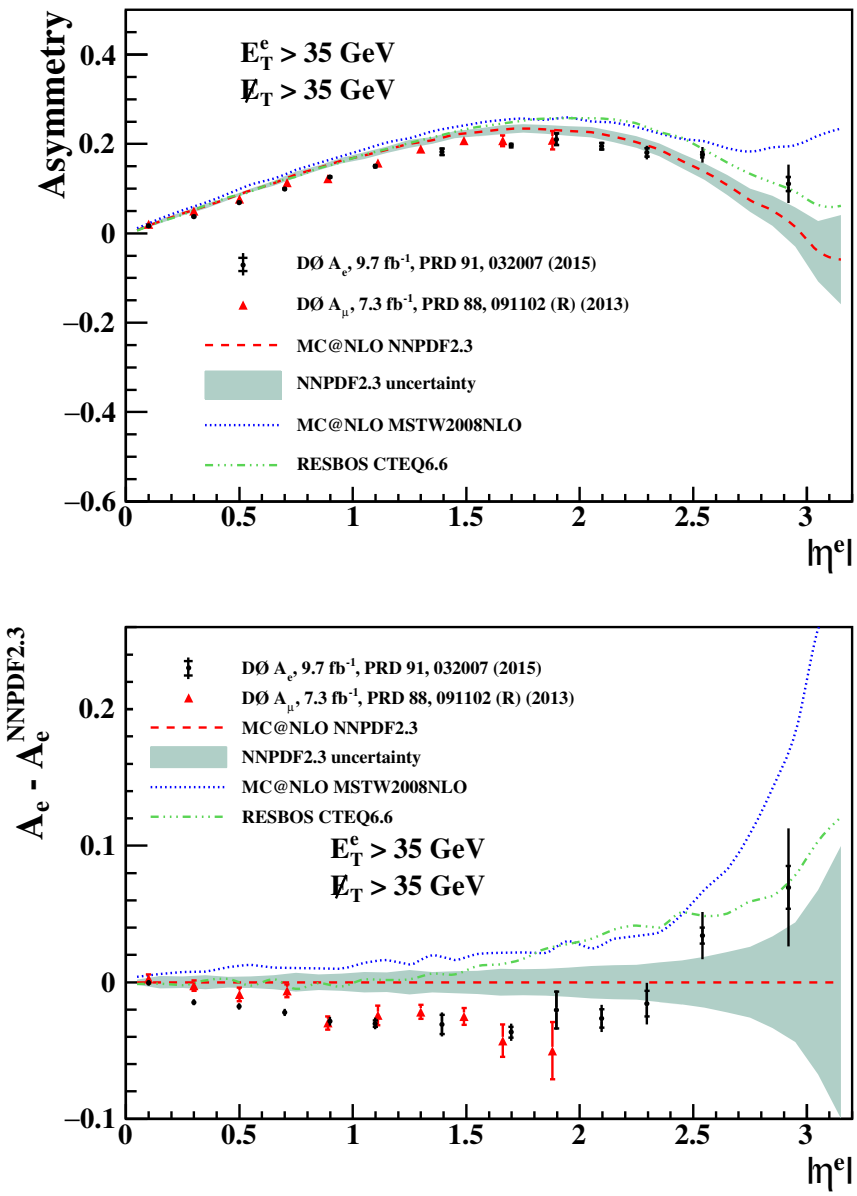

FIG. 4: The electron charge asymmetry distribution after CP folding with symmetric kinematic cuts $E_T^e > 35$ GeV, $\not{E}_T > 35$ GeV. (top) Comparison between the measured asymmetry and predictions and (bottom) the differences between the data and MC predictions and the predicted central value from MC@NLO using the NNPDF2.3 PDF set. The black dots show the measured electron charge asymmetry, with the horizontal bars showing statistical uncertainty and the vertical lines showing the total uncertainty. The red up-pointing triangles show the D0 muon charge asymmetry. The red dashed lines and cyan bands are the central value and uncertainty band from MC@NLO using the NNPDF2.3 PDF sets. The blue dotted lines show the prediction from MC@NLO using the MSTW2008NLO central PDF set, and the green dot-dashed lines show the prediction from RESBOS using the CTEQ6.6 central PDF set.

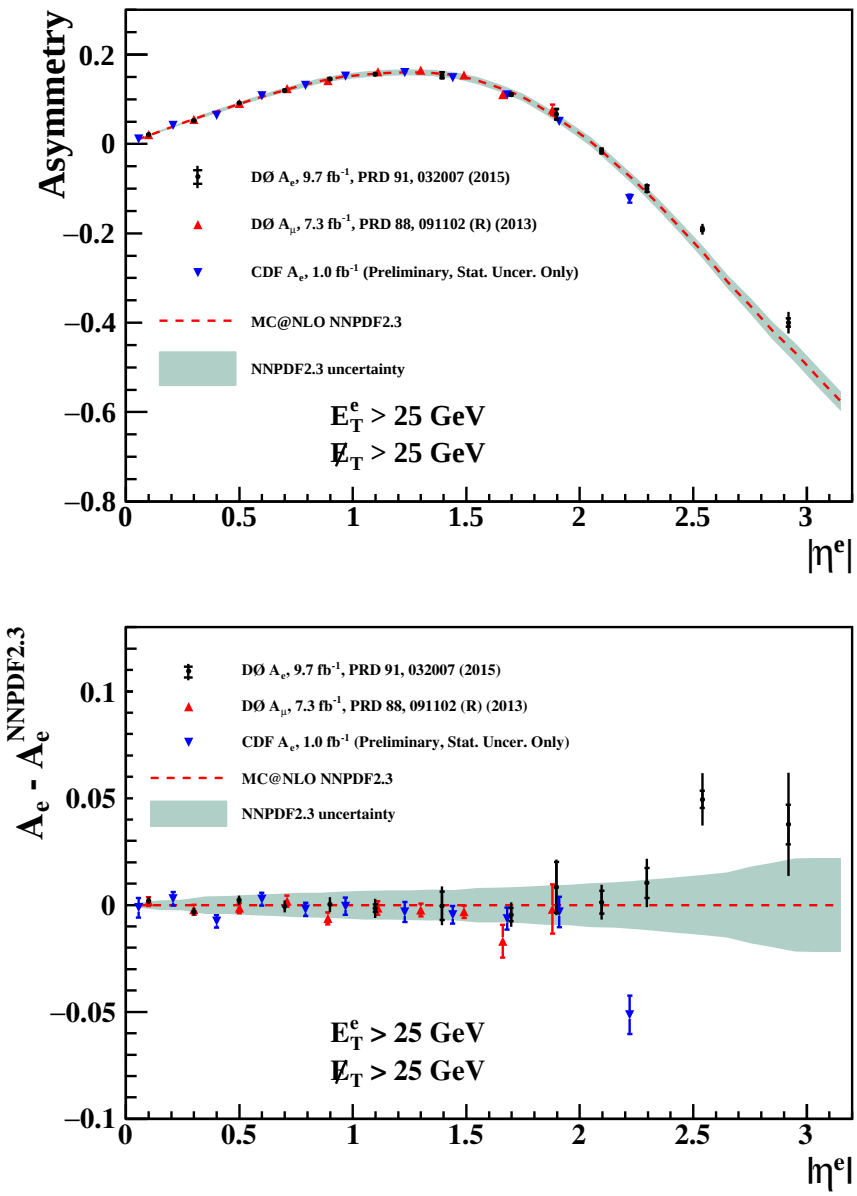

FIG. 5: The electron charge asymmetry distribution after CP folding with symmetric kinematic cuts $E_T^e > 25$ GeV, $\not{E}_T > 25$ GeV. (top) Comparison between the measured asymmetry and predictions and (bottom) the differences between the data and MC predictions and the predicted central value from MC@NLO using the NNPDF2.3 PDF set. The black dots show the measured electron charge asymmetry, with the horizontal bars showing statistical uncertainty and the vertical lines showing the total uncertainty. The red up-pointing triangles show the D0 muon charge asymmetry, the blue down-pointing triangles show the CDF electron charge asymmetry. The red dashed lines and cyan bands are the central value and uncertainty band from MC@NLO using the NNPDF2.3 PDF sets.

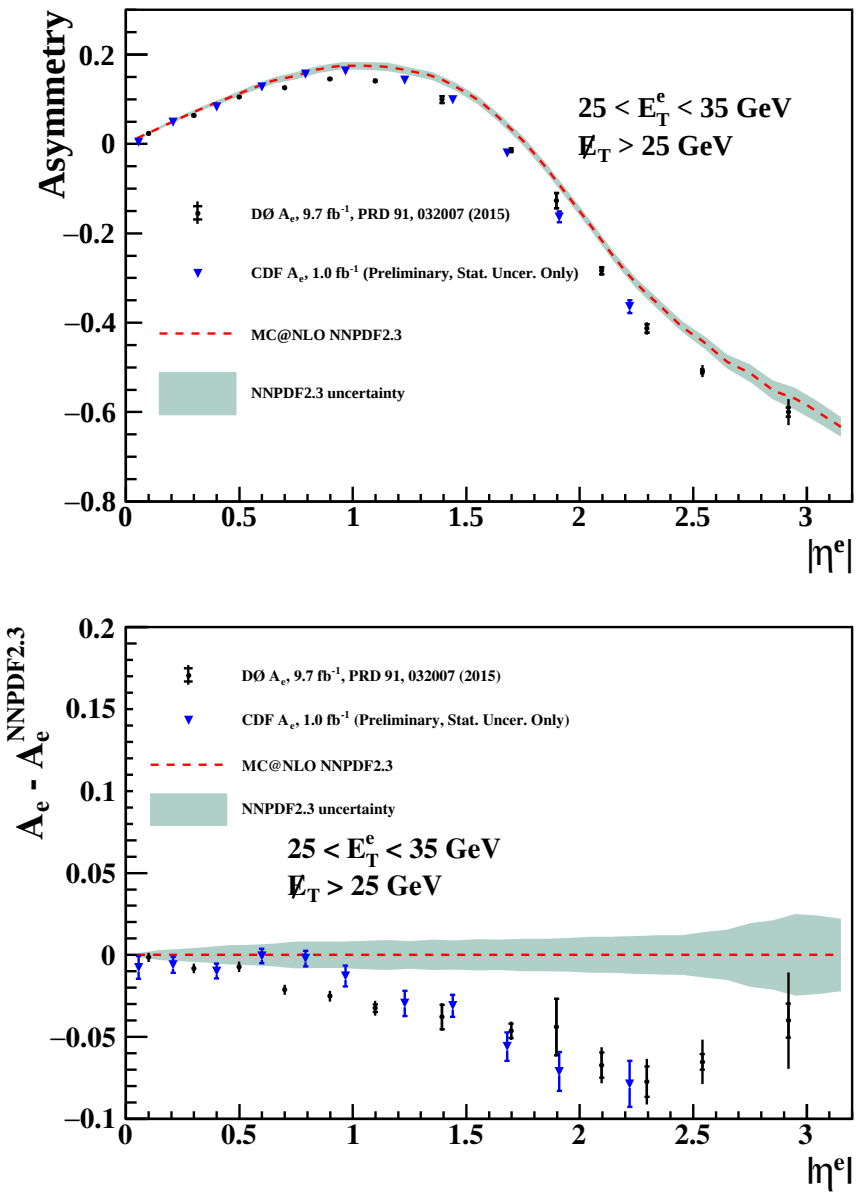

FIG. 6: The electron charge asymmetry distribution after CP folding with symmetric kinematic cuts $25 < E_T^e < 35$ GeV, $\not{E}_T > 25$ GeV. (top) Comparison between the measured asymmetry and predictions and (bottom) the differences between the data and MC predictions and the predicted central value from MC@NLO using the NNPDF2.3 PDF set. The black dots show the measured electron charge asymmetry, with the horizontal bars showing statistical uncertainty and the vertical lines showing the total uncertainty. The blue down-pointing triangles show the CDF electron charge asymmetry. The red dashed lines and cyan bands are the central value and uncertainty band from MC@NLO using the NNPDF2.3 PDF sets.

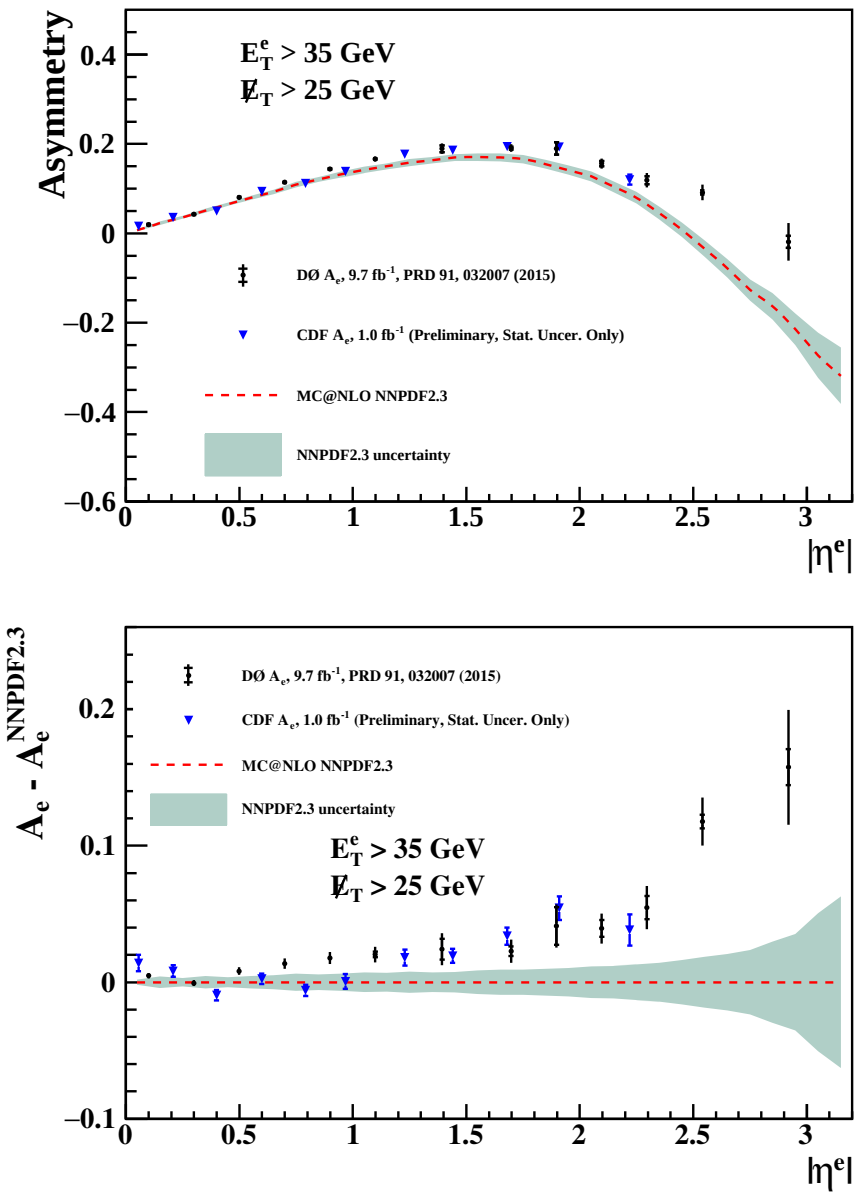

FIG. 7: The electron charge asymmetry distribution after CP folding with symmetric kinematic cuts $E_T^e > 35$ GeV, $\not{E}_T > 25$ GeV. (top) Comparison between the measured asymmetry and predictions and (bottom) the differences between the data and MC predictions and the predicted central value from MC@NLO using the NNPDF2.3 PDF set. The black dots show the measured electron charge asymmetry, with the horizontal bars showing statistical uncertainty and the vertical lines showing the total uncertainty. The blue down-pointing triangles show the CDF electron charge asymmetry. The red dashed lines and cyan bands are the central value and uncertainty band from MC@NLO using the NNPDF2.3 PDF sets.

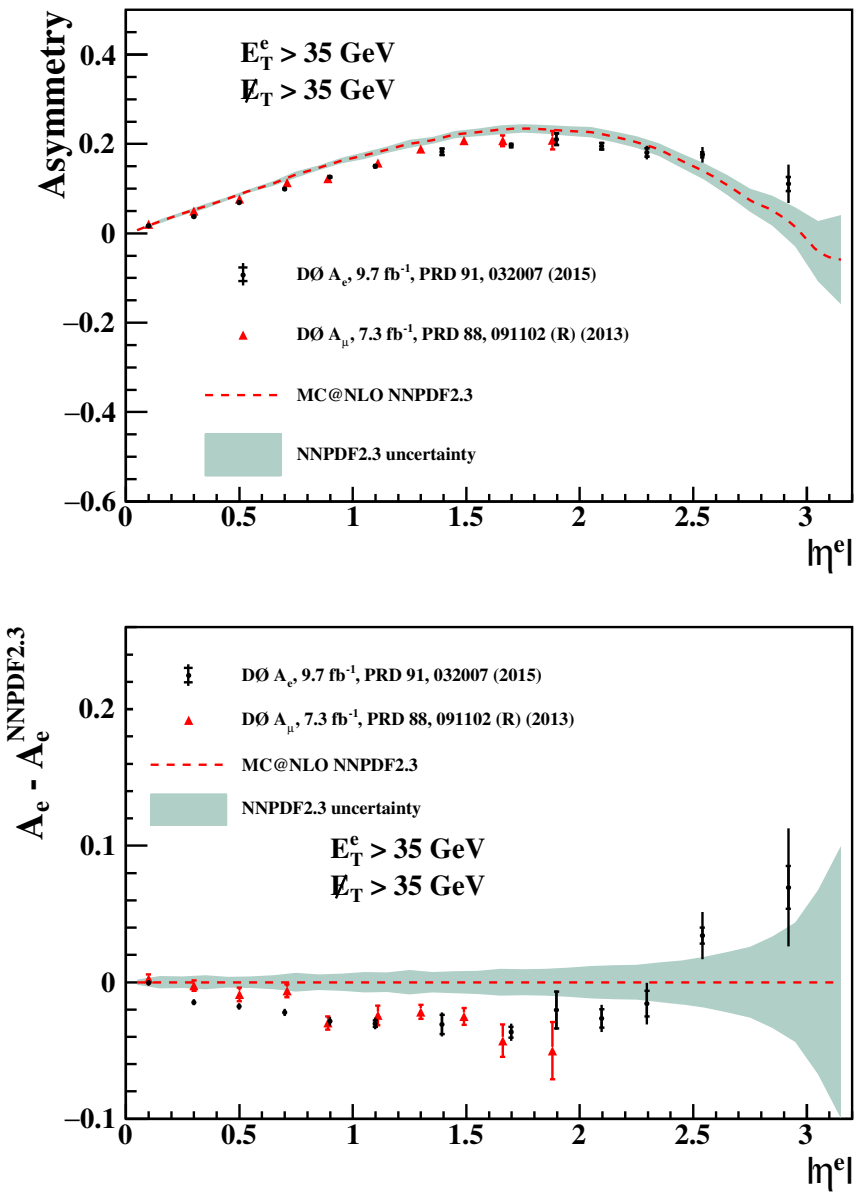

FIG. 8: The electron charge asymmetry distribution after CP folding with symmetric kinematic cuts $E_T^e > 35$ GeV, $\not{E}_T > 35$ GeV. (top) Comparison between the measured asymmetry and predictions and (bottom) the differences between the data and MC predictions and the predicted central value from MC@NLO using the NNPDF2.3 PDF set. The black dots show the measured electron charge asymmetry, with the horizontal bars showing statistical uncertainty and the vertical lines showing the total uncertainty. The red up-pointing triangles show the D0 muon charge asymmetry. The red dashed lines and cyan bands are the central value and uncertainty band from MC@NLO using the NNPDF2.3 PDF sets.